ACS NANO

www.acsnano.org

ARTICLE

Designing Core–Shell Gold and Selenium Nanocomposites for Cancer Radiochemotherapy

Yanzhou Chang,[†] Lizhen He,[†] Zhibin Li,[‡] Lilan Zeng,[†] Zhenhuan Song,[†] Penghui Li,[‡] Leung Chan,[‡] Yuanyuan You,[†] Xue-Feng Yu,*[,‡] Paul K. Chu,[§] and Tianfeng Chen*[,†]

[†]Department of Chemistry, Jinan University, Guangzhou 510632, P.R. China

[‡]Institute of Biomedicine and Biotechnology, Shenzhen Institutes of Advanced Technology, Chinese Academy of Sciences, Shenzhen 518055, P.R. China

[§]Department of Physics and Materials Science, City University of Hong Kong, Tat Chee Avenue, Kowloon, Hong Kong, China

Supporting Information

ABSTRACT: **Radiotherapy is an important regime for treating malignant tumors. There is interest in the development of radiosensitizers to increase the local treatment efficacy under a relatively low and safe radiation dose. In this study, we designed Au@Se-R/A nanocomposites (Au@Se-R/A NCs) as nanoradiosensitizer to realize synergistic radiochemotherapy based on the radiotherapy sensitization property of Au nanorods (NRs) and antitumor activity of Se NPs. *In vitro* studies show that the combined treatment of A375 melanoma cells in culture with NCs and X-ray induces cell apoptosis through alteration in expression of p53 and DNA-damaging genes and triggers intracellular ROS overproduction, leading to greatly enhanced anticancer efficacy. Further studies using clinically used radiotherapy equipment demonstrate that the combined treatment of NCs and X-ray significantly inhibits the tumor growth *in vivo* and shows negligible acute toxicity to the major organs. Taken together, this study provides a strategy for clinical translation application of nanomedicne in cancer radiochemotherapy.**

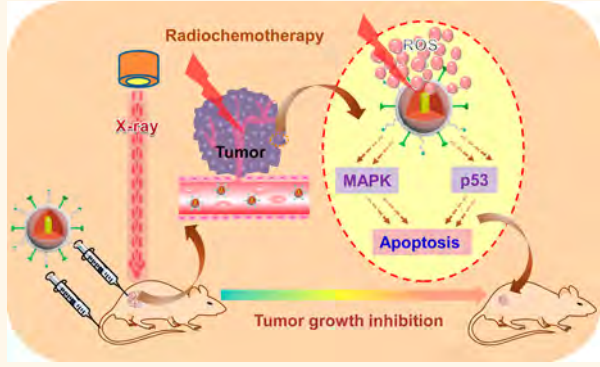

KEYWORDS: *nanocomposites, targeting, radiochemotherapy, radiosentization, cancer therapy*

Radiotherapy and chemotherapy are two of the most commonly used cancer treatment methods, but their therapeutic efficacy is plagued by dose-limiting radiation and drug toxicity. Interestingly, drugs with the safe dosage may not cure the patients completely.[1−6] For example, the radiotherapy effect is seriously limited by the radiation resistance of hypoxic cells in some tumors, and an excessive radiation dose may damage surrounding healthy tissues and produce other toxic side effects.[2,3,7,8] As a result, tumors may not be fully eradicated, resulting in possible tumor recurrence and metastasis. Although some chemical radiosensitizers have been suggested to accentuate the effects of radiotherapy, there is a need to develop a sensitizer that can optimize the radiotherapy efficacy at a lower effective dose and act as a chemotherapy drug to inhibit tumor cell proliferation.[9,10]

High-*Z* (high atomic number) nanomaterials with enhanced photoelectric and Compton effects have aroused much interest because of possible enhancement of the therapeutic efficiency and specificity of radiotherapy.[10−12] Gold nanoparticles (Au NPs) with an atomic number *Z* of 79 have strong photoelectric absorbance, low toxicity, high stability, and multifunctionality.[13] Hainfeld *et al.* employed Au NPs to enhance the radiotherapy of tumor in mice.[14,15] Misawa *et al.* discovered that radiosensitization relied on the enhanced generation of reactive oxygen species (ROS) by Au NPs under X-ray irradiation.[16] Zhang *et al.* reported that glutathione (GSH) modification could help Au NPs to deposit in tumors, leading to better safety and efficacy of radiotherapy.[17] In addition, the multifunctionality of Au NPs with different morphologies renders them popular in other cancer treatment applications such as photothermal therapy and photodynamic therapy.[18−24]

To integrate radiotherapy and chemotherapy, a Au-based nanocomposite (NC), core–shell structured Au@Se NC, is

Received: February 25, 2017
Accepted: May 1, 2017
Published: May 1, 2017

DOI: 10.1021/acsnano.7b01346
ACS Nano 2017, 11, 4848−4858

synthesized and evaluated in this work. Se NPs have been studied by some groups including ours and proposed as an efficient anticancer nanoagent and drug carrier.[25−27] We have recently reported that conjugation of cancer-targeting units improves the stability and anticancer efficacy of Se NPs,[26,28,29] and smart decoration of Se NPs can produce sequentially triggered drug release, precise drug delivery, and simultaneous inhibition of cancer growth, migration, and invasion.[29] Here, we synthesized a Au@Se NC that combines Au nanorods (NRs) and Se NP. We hypothesize this composite nanomaterial can act as a nanosensitizer for synergistic cancer radiochemotherapy. The overall design for the nanocomposite and their application is described in Scheme 1. Taken together, this study provides a strategy for clinical translation application of nanomedicne in cancer radiochemotherapy.

Scheme 1. Schematic Illustration Au@Se-R/A NCs Can Be Exploited To Synergistically Enhance the Radiochemotherapy Effect

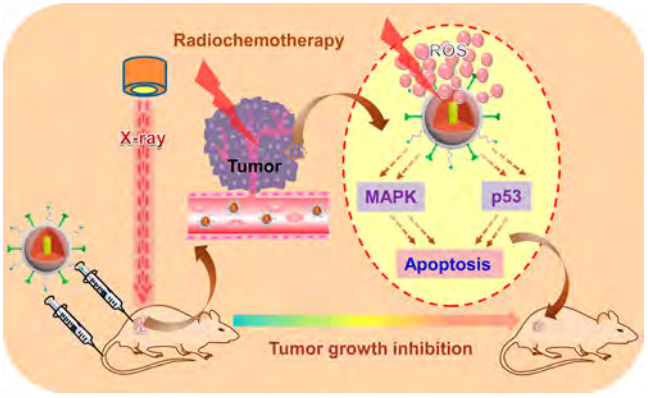

RESULTS AND DISCUSSION

Synthesis and Characterization Structure of Au@Se-R/A (R/A: RGD/ACPP) NCs. The synthesis protocol is outlined in Figure 1A, and the characterization results are shown in Figure 1B−K and Figures S1 and S2. The Au NRs synthesized by a seed-mediated growth method[30,31] exhibit a regular rod shape with the length and width of 61 ± 6 and 17 ± 2 nm, respectively (Figure 1B). After Se shell formation and conjugation, the Au@Se-R/A NCs show a spherical morphology with a uniform size of about 120 nm (Figure 1C). High-resolution transmission electron microscopy (TEM) shows that the polymer envelops the NCs (Figure 1D). The high-angle annular dark-field scanning TEM (HAADF-STEM) and TEM energy-dispersive X-ray spectrometry (TEM-EDS) line profiles in Figure 1E,F reveal the elemental distribution in the Au core and Se shell and confirm the formation of the Au@Se core−shell nanostructure.

The products during the synthesis process are examined. The ζ-potential analysis in Figure 1G shows that the Au NRs are positively charged (19.3 mV) and Se NPs are negatively charged (−7.4 mV), thus facilitating shell wrapping. The Au@Se NCs are modified with positively charged chitosan (CS), and the potential changes from −6.3 to +26.9 mV. From the results of Fourier transform infrared (FT-IR) spectroscopic analysis (Figure 1H), the presence of characteristic peaks of CS and the targeting peptides in Au@Se-R/A NCs further confirms their successful conjugation to the surface of the Se shells. Moreover, the coupling amount of RGD[32,33] and ACPP[34,35] is 19.35 and 16.59 μg/mg, respectively.

The optical absorption properties are used to determine shell formation and molecule conjugation (see Figure 1I,J). The original Au NRs show the typical longitudinal surface plasmon resonance (LSPR) band at about 760 nm, whereas the pure Se NPs show no absorption band. After shell formation and CS modification, the LSPR peak wavelength of the Au@Se NPs red-shifts to about 1113 nm because of the increase in the refractive index of the surrounding medium,[31,36] and the solution color changes from lilac to reddish brown. After conjugation with RGD/ACPP molecules, the LSPR peak wavelength further red-shifts to about 1123 nm.

The stability of the Au@Se-R/A NCs in the biological environment is evaluated by examining the size change (Figure 1K and Figure S1). When they are dispersed in water, 10% FBS in DMEM and serum for more than 168 h, no obvious size change can be found, thereby revealing good stability in biological media, boding well for subsequent *in intro* and *in vivo* experiments.

Au@Se-R/A NCs Synergistically Enhance the Anticancer Efficacy of X-ray. *In vitro* experiments are performed to determine the radiotherapy-enhancing effects of the Au@Se-R/A NCs. A375 melanoma cells as typical hypoxic and malignant cancer cells are employed due to their strong radio-resistance ability (Figure S2).[37−39] As shown in Figure 2A and Table S1, during individual drug treatment, the IC_{50} value of Se NCs is 39.1 μM, whereas that of Au@Se NCs decreases to 21.0 μM (as calculated by Se). As calculated by Au, the IC_{50} value of Au NRs is 7.7 μM and decreases significantly to 0.49 μM for Au@Se NCs (Table S2). These results clearly show that the Au@Se NCs can reduce the drug dose used in cancer radiotherapy. To further improve the selectivity of the nanodrugs to tumor cells, two kinds of tumor-cell-targeting peptides (RGD and ACPP) are employed. The RGD peptide can recognize the $\alpha v\beta 3$ integrin receptor overexpressed in various human cancer cells,[40,41] and ACPP peptide can be site-specifically cleaved by matrix metalloproteinases MMP-2/9 at the tumor extracellular matrix. Therefore, it is expected that the NCs with grafted polycationic CPP can more easily penetrate cell membranes to improve uptake by tumor cells.[34,42−44] As shown in Figure 2A, the Au@Se NCs grafted with either the RGD- or ACPP-targeting peptide increases the lethality. Especially for the dual-targeting Au@Se-R/A NCs, the IC_{50} value drops to 10.89 μM (calculated by Se), which is smaller than those of Au@Se-R NCs (18.78 μM) and Au@Se-A NCs (16.27 μM). Dose-dependent radiochemotherapy is further preformed to examine the antitumor activity of the Au@Se-R/A NCs with dual-targeting peptide conjugation. Under 8 Gy irradiation, the IC_{50} value of Au@Se-R/A NCs decreases to 1.06 μM, and this is 10 times smaller than that in a single peptide treatment. Table S3 illustrates that the Au@Se-R/A NCs have satisfactory biological safety by virtue of relatively high safety index (SI), and the morphology of the Au@Se-R/A NCs does not change despite X-ray (4 Gy) irradiation (Figure S3), demonstrating X-ray stability.

The cell uptake ability of the Au@Se-R/A NCs by human cancer and normal cells is examined. As shown in Figure 2B, the Au@Se-R/A NCs with peptide conjugation exhibit cell uptake in A375 human cancer cells higher than that of the Au@Se NCs. The uptake of Au@Se-R/A NCs increases in a time- and dose-dependent manner (Figure S5), and the uptake amounts by A375 cancer cells are more than twice that of L02

DOI: 10.1021/acsnano.7b01346
ACS Nano 2017, 11, 4848−4858

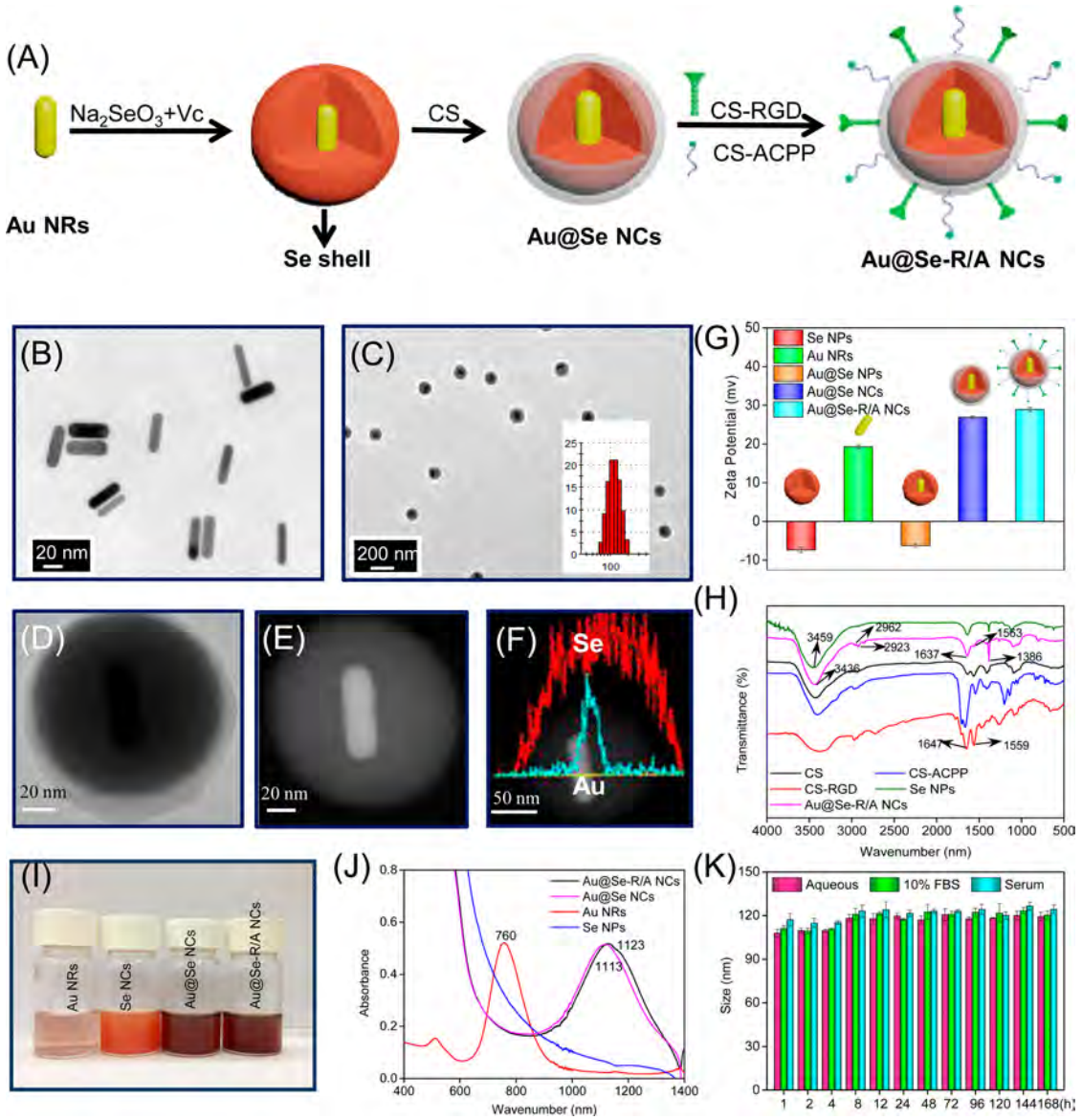

Figure 1. Schematic illustration of the synthesis of Au@Se-R/A NCs and structure of the product: (A) Schematic illustrating of the Au@Se-R/A NCs. (B) TEM image of Au NRs. (C) TEM image with inset showing hydrodynamic size distribution of Au@Se-R/A NCs. (D) High-magnification TEM image of one Au@Se-R/A NC. (E) HAADF-STEM image of one Au@Se-R/A NC. (F) Image of linear TEM-EDS of one Au@Se-R/A NC. (G) ζ-Potential of different products in the synthesis. (H) FT-IR spectra of CS, Se NPs, CS-RGD, CS-ACPP, and Au@Se-R/A NCs. (I) Digital photographs and (J) absorption spectra of Au NRs, Se NPs, Au@Se NCs, and Au@Se-R/A NCs. (K) Changes in the hydrodynamic size of Au@Se-R/A NCs in water, 10% FBS, and human FBS. Each value represents means ± SD (n = 3). Bars with different characteristics are statistically different at the $P < 0.05$ level.

normal cells (8 h) (Figure 2C). The results demonstrate that RGD/ACPP conjugation enhances selective cellular uptake and anticancer efficacy.

Isobologram analysis is employed to determine the interaction between X-ray and Au@Se-R/A NCs. As shown in Figure 2D, the inhibitory effect of X-ray and NCs on A375 cells is synergistic, as evidenced by the fact that data points in the isobologram are far below the line defining the additive effect.[45] In addition, our results also demonstrated the synergistic interaction between Au NRs and Se NPs (Figure S4). Intracellular trafficking of the NCs in A375 cells is also monitored, and as shown in Figure 2E, the Au@Se-R/A NCs (green fluorescence) move across the cell membrane after treatment for 2 h. The NCs are located continuously and accumulated in lysosomes until 4 h and finally fill the whole cytoplasm after 6 h, indicating that lysosome is the main target organelle of the Au@Se-R/A NCs. Receptor-mediated endocytosis may be the major mechanism responsible for selective cellular uptake of the NCs.

Multicellular tumor spheroids (MCTS) are a conventional *in vitro* tumor three-dimensional (3D) cell culture model and simulating drug and nanoparticle transport in tumors.[46−48] In this study, A375 MCTS serves as the tumor model to compare the penetration ability of the nanosystems (Figure 2F). As shown in Figure 2G, compared to Au@Se NCs, the Au@Se-R/A NCs show deeper penetration reaching the central region of the A375 MCTS. The A375 MCTS volume ratios are computed after treatment with the Au NRs, Se NCs, Au@Se NCs, and Au@Se-R/A NCs. As shown in Figure 2H,I, the Au@

DOI: 10.1021/acsnano.7b01346
ACS Nano 2017, 11, 4848−4858

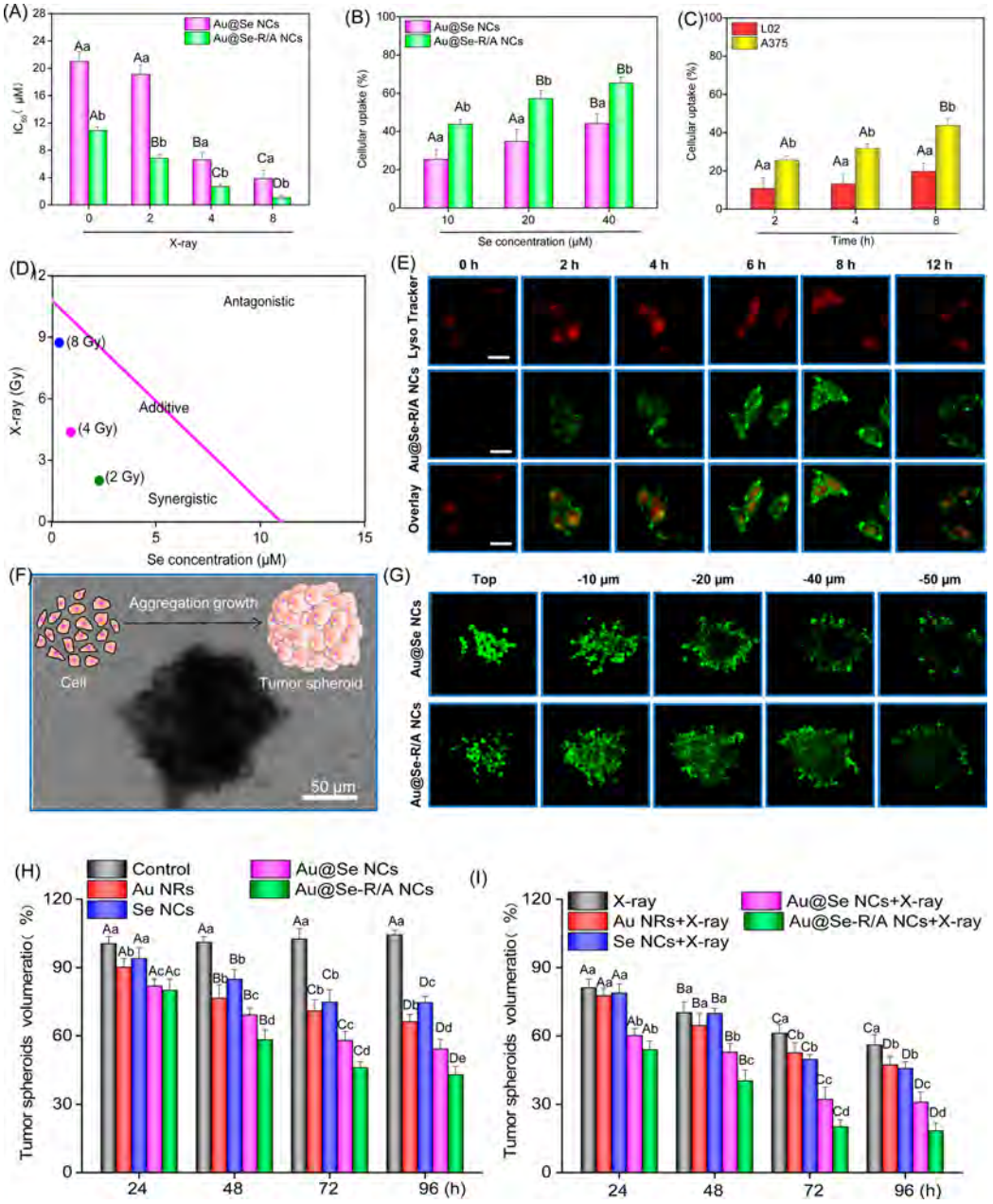

Figure 2. Enhanced X-ray anticancer efficacy and cellular uptake: (A) Cytotoxic effects of Au@Se NCs and Au@Se-R/A NCs on A375 cells after incubation for 72 h. (B) Quantitative analysis of the cellular uptake efficiency of coumarin-6-loaded Au@Se NCs and Au@Se-R/A NCs in A375 cells at different concentrations after incubation for 8 h. (C) Selective uptake of Au@Se-R/A NCs (10 μM) by L02 cells and A375 cells. (D) Isobologram analysis of the synergistic antiproliferative effect of the combined application of X-ray and Au@Se-R/A NCs on A375 cells. The data points in the isobologram correspond to the growth inhibition ratio at 50% in the combined treatment. (E) Intracellular trafficking of coumarin-6-loaded Au@Se-R/A NCs in A375 cells. The cells are treated with coumarin-6-loaded Au@Se-R/A NCs (20 μM) for different periods of time and stained with LysoTracker (red fluorescence, lysosome). The scale bar is 20 μm. Original magnification 20×. (F) Formation model of MCTS and optical microscopic images of A375 MCTS. (G) Penetrating ability of Au@Se NCs (10 μM) and Au@Se-R/A NCs (10 μM) into A375 MCTS. The MCTS are treated with coumarin-6-labeled nanoparticles for 8 h. (H,I) Inhibitory effects of Au NRs (0.3 μM), Se NCs (10 μM), Au@Se NCs (10 μM), and Au@Se-R/A NCs (10 μM) with or without X-ray on A375 MCTS. Upper case letters indicate significant differences at $P < 0.05$ level between groups, and lower case letters indicate significant differences at $P < 0.05$ level within groups. Each value represents means ± SD ($n = 3$).

Se-R/A NCs repress growth of the A375 MCTS, especially under the conditions of radiochemotherapy.

Anticancer Action Mechanisms of Au@Se-R/A NCs to A375 Cells. The mechanism of the radiosensitization effects of the Au@Se-R/A NCs is investigated. The possible signaling pathway triggered by the NCs and X-ray is shown in Figure 3A. As revealed by flow cytometry (Figure 3B), X-ray alone causes 5.6% cell apoptosis, and the Au@Se-R/A NCs (from 2 to 8 μM) increase cell death from 16.4 to 36.9%, as shown by the increase in the sub-G1 cell proportion. The combination of Au@Se-R/A NCs and X-ray increases the sub-G1 proportion further. For instance, Au@Se-R/A NCs (8 μM) and X-ray increase of the sub-G1 peak to 43.6% and combination of X-ray and Au NRs (0.2 μM), Se NCs (8 μM), and Au@Se NCs (8

DOI: 10.1021/acsnano.7b01346
ACS Nano 2017, 11, 4848−4858

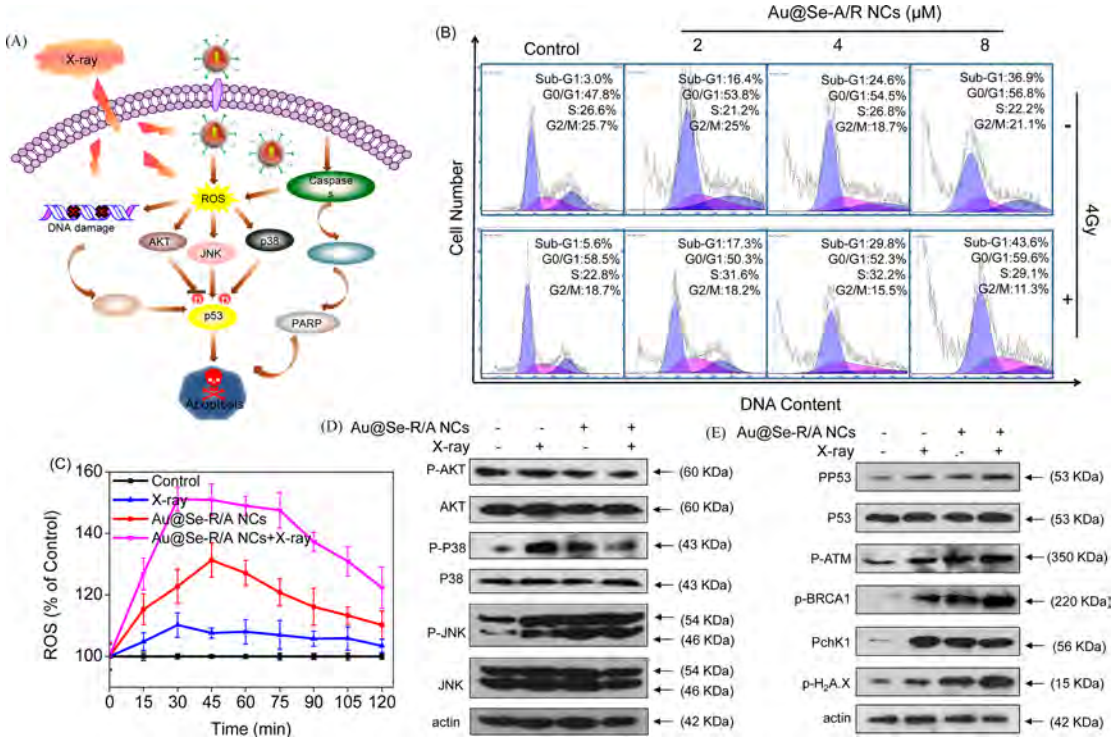

Figure 3. Anticancer action mechanism of Au@Se-R/A NCs to A375 cells. (A) Signaling pathways triggered by Au@Se-R/A NCs and X-ray. (B) Flow cytometric analysis of A375 cells after introduction Au@Se-R/A NCs with (+) or without (−) X-rays (4 Gy). (C) Overproduction of superoxide in A375 cells treated with Au@Se-R/A NCs (32 μM) with (+) and without (−) X-ray (4 Gy). (D) Effects of Au@Se-R/A NCs (20 μM) with (+) and without (−) X-ray (4 Gy) on the phosphorylation status and expression levels of MAPKs and AKT pathways. (E) Au@Se-R/A NCs (20 μM) enhancing X-ray apoptosis by triggering p53 phosphorylation. Each value represents means ± SD (n = 3). Bars with different characteristics are statistically different at the $P < 0.05$ level.

μM) increases cell apoptosis to 7.0, 18.0, and 28.5% (Figure S6). The results indicate synergistic anticancer action through promotion of cell apoptosis, in which caspase family members play a critical role.[45,49,50] Se NPs also show anticancer effects by caspase-mediated apoptosis in different cancer cells.[25,26,29] Therefore, the expression levels of caspase family and other related proteins are determined by Western blotting. As shown in Figure S7, exposure of A375 cells to Au@Se-R/A NCs and X-ray activates caspase-3/-8/-9 as well as poly-ADP-ribose polymerase (PARP) cleavage, providing more evidence about that the synergistic effects of the combined treatment arising from the caspase-mediated apoptotic pathway.

Radiotherapy can induce overproduction of reactive oxygen species (ROS), including hydroxyl radicals, superoxide anions, and hydrogen peroxide, to cause DNA damage and cell death, and generation of intracellular ROS is examined by the DCFH-DA probe in the cell and cell-free models. As shown in Figure S8, the Au NR treatment and Se NC treatment increase the ROS level slightly, and in spite of using X-ray together, the content of ROS is not altered significantly. In contrast, as shown in Figure 3C, the Au@Se-R/A NCs increase the ROS level to 131% within 45 min in the cell model, and the combined application of Au@Se-R/A NCs and X-ray treatment increases the ROS content to 151% within 30 min. ROS overproduction in interactions between X-ray NCs in the cell free model is also described in Figure S8. The results indicate that the Au@Se-R/A NCs and X-ray elevate ROS generation synergistically.

The downstream signaling pathway of ROS overproduction produced by the combined treatment is explored. The AKT signaling pathway is essential to cell proliferation, differentiation, and apoptosis, and the expression and phosphorylation of AKT in A375 cells treated with X-ray and Au@Se-R/A NCs are determined. As shown in Figure 3D, the combined treatment up-regulates the expression of phosphorylated p38 and JNK, and phosphorylation of AKT declines slightly after radiochemotherapy. The p53 is an important tumor suppressor gene responsible for oxidative stress and directly or indirectly induces cell apoptosis. Western blotting is employed to examine the combined effects on the expression of p53 and DNA damage-related proteins in A375 cells. As expected, the combined treatment increases DNA damage (Figure 3E) by elevating the phosphorylation levels of ATM, chk2, p-BRCA1, p53, and histone. Moreover, the Au@Se-R/A NCs and X-ray synergistically activate the AKT, p53, and DNA damage-related signaling pathway to suppress tumorigenesis. Taken together, these results suggest that the ROS-mediated signaling pathways may play an important role in the anticancer action of the core−shell Au@Se nanocomposites.

***In Vivo* Therapeutic Effects and Biodistribution of Au@Se-R/A NCs in A375-Bearing Mice.** The *in vivo* radiotherapy sensitization efficacy after intravenous (IV) and introtumor (IT) injection is analyzed using A375 subcutaneous transplanted tumor-bearing nude mice. Owing to the good near-infrared photoacoustic properties of Au NRs,[24,51,52] the Au@Se-R/A NCs are used as an exogenous contrast agent in *in vivo* photoacoustic imaging to determine the accumulation time in the tumor. The Au@Se-R/A NCs reach the tumor region after 2 h and appear to accumulate inside the entire tumor 6 h after IV injection (Figure S9). Therefore, the time point of 6 h

DOI: 10.1021/acsnano.7b01346
ACS Nano 2017, 11, 4848−4858

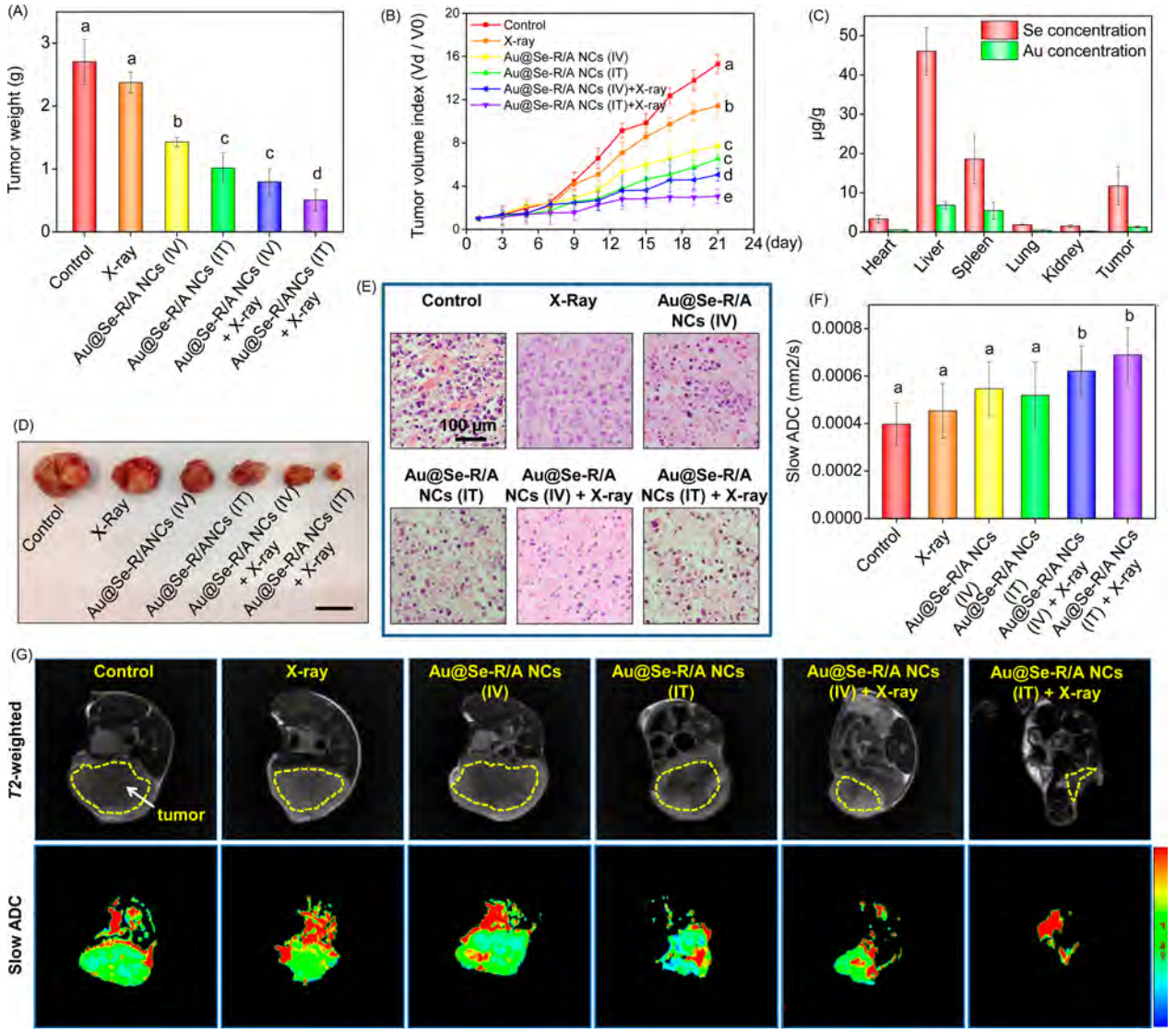

Figure 4. *In vivo* **therapeutic effects and biodistribution of Au@Se-R/A NCs in A375-bearing mice. (A) Tumor weight of tumor-bearing mice at 21 days. (B) Tumor volume index for different treatment in 21 days. (C)** *In vivo* **biodistribution of Au@Se-R/A NCs (IV). (D) Photographs of tumors collected from different groups of mice 21 days after the treatment (scale bar: 1 cm). (E) Histological analysis of the tumors in mice following different treatments. (F) Quantitative analysis of the pseudocolor signals of slow ADC. (G) T_2-weighted MR images and slow ADCs of A375 tumor-bearing mice after different treatments after 21 days. The tumor sites are in the back region and circled by dashed lines. Each value represents means ± SD (n = 3). Bars with different characteristics are statistically different at the P < 0.05 level.**

is adopted in the subsequent radiation therapy study. As expected, the radiotherapy alone treatment (group 2) does not inhibit tumor growth (Figure 4A,B), and the Au@Se-R/A NCs (IV) (group 3) and Au@Se-R/A NCs (IT) (group 4) only inhibit tumor growth slightly. However, the Au@Se-R/A NCs (IV) + X-ray (group 5) and Au@Se-R/A NCs (IT) + X-ray (group 6) inhibit tumor growth more effectively. The therapeutic efficacy observed from group 5 (IV) is a little lower than that of group 6 (IT). The biodistribution of the Au@Se-R/A NCs in different tissues is determined (Figure 4C), and the Au@Se-R/A NCs (IV) accumulate mainly in the liver, spleen, and tumor. The body weight of the animals during the treatment period does not fluctuate drastically for the different treatments (Figure S10), suggesting that the treatment is tolerated, causing no acute side effects during cancer therapy. The photographs of the dissected tumors and tumor size are consistent with the caliper measurements (Figure 4D). The therapeutic effect producd by the combined Au@Se-R/A NCs and X-ray can be attributed to, by absorbing X-ray, the Au atoms producing photons to damage DNA and generating ROS to kill tumor cells.

The histological changes in the tumors are recorded to evaluate the antitumor efficacy of the Au@Se-R/A NCs by hematoxylin and eosin (H&E) staining. As shown in Figure 4E, the mice in the control group show no obvious cell apoptosis, and those in groups 3 and 4 show moderate tumor cell apoptosis. In comparison, groups 5 and 6 show obvious tumor damage and irregular widening of intercellular space.

As a means to examine tissue lesion,[10] T_2-weighted magnetic resonance (MR) imaging is more sensitive to bleeding, and the signal can be enhanced by the emergence of tissue edema during the treatment. Therefore, MR imaging is performed to examine the changes of the tumor status. As shown in Figure 4F,G, larger slow ADC signals (red color) are observed from the tumors in groups 5 and 6, indicating smaller cancer cell densities inside the tumors and a larger degree of tumor cell

DOI: 10.1021/acsnano.7b01346
ACS Nano 2017, 11, 4848−4858

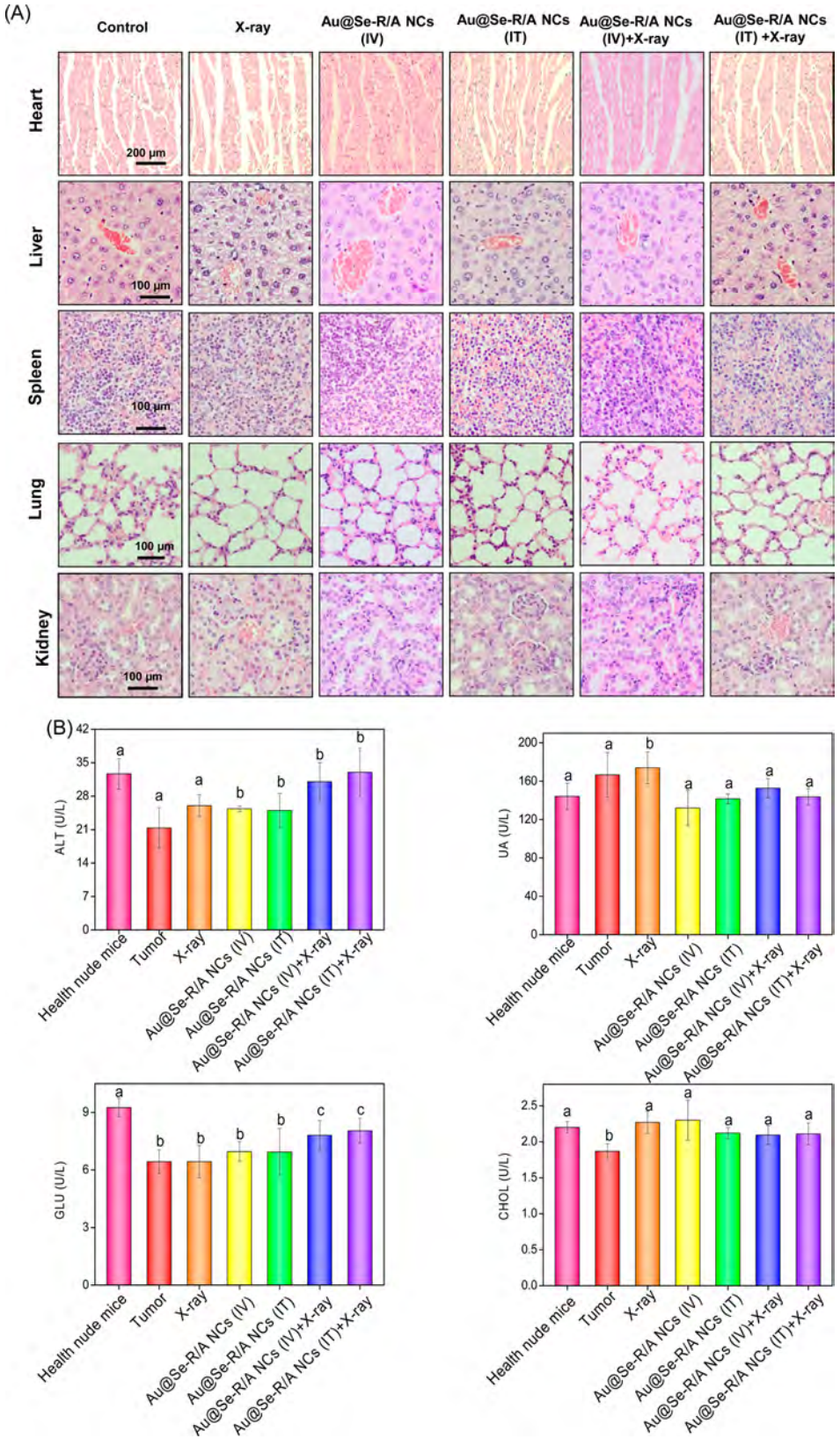

Figure 5. ***In vivo*** **toxicity evaluation. (A) H&E-stained slice images of major organs. Each value represents means ± SD (*n* = 3), and bars with different characteristics are statistically different at the *P* < 0.05 level. (B) Blood biochemistry data including liver function markers, ALT; kidney function markers, UA; blood glucose, GLU; and blood fat, CHOL.**

death. The increase in the T_2-weighted signal indicates more apoptotic cell death in groups 5 and 6, and more inhibiton of the tumor volume is observed from these two groups, as well.

In Vivo **Toxicity Evaluation.** To study the potential side effects of the Au@Se-R/A NCs, the main organs of mice are collected and subjected to H&E staining. As shown in Figure

DOI: 10.1021/acsnano.7b01346
ACS Nano 2017, 11, 4848−4858

5A, no obvious impairment or inflammation is found compared to the control groups despite the high levels of the Au@Se-R/A NCs accumulating in the liver and spleen after IV injection for the tested dose range. Blood biochemical tests are conducted to monitor the major organs after the treatment, and as shown in Figure 5B, the levels of alanine aminotransferase (ALT), uric acid (UA), blood glucose (GLU), and cholesterol (CHOL) (index for function of liver, kidney, blood glucose, and blood fat) in the Au@Se-R/A NCs + X-ray groups are similar to those of healthy mice, demonstrating the safety of the radiotherapy.

CONCLUSION

Au@Se-R/A NCs are designed and prepared to serve as a nanosensitizer for achieving highly efficient synergistic cancer radiochemotherapy. The NCs exhibit tumor-targeting capability, cellular uptake, radiosensitization ability, and enhanced radiotherapy-induced tumor destruction. The combined application of the NCs and X-ray induces cancer cell apoptosis *via* change in p53 expression and proteins that are related to damaging DNA and caused intracellular ROS overproduction. *In vivo* radiotherapy studies demonstrate that the combined application of the NCs and X-ray inhibits tumor growth while showing negligible acute toxicity.

EXPERIMENTAL SECTION

Materials. Sodium selenite (Na_2SeO_3), *N*-succinimidyl-3-maleimidopropionate (SMP), chitosan (CS), 1-ethyl-3-[3-(dimethylamino)-propyl]carbodiimide hydrochloride (EDC), *N*-hydroxysuccinimide (NHS), and L-ascorbic acid (Vc) were purchased from Sigma–Aldrich. The caspase substrates were purchased from Calbiochem. All the chemicals were used as received.

Characterization. Transmission electron microscopy, dark-field scanning TEM (DF-STEM), energy-dispersive X-ray spectrometry (EDS), and linear TEM-EDS were carried out on the JEOL-2100F TEM at an acceleration voltage of 200 kV. The dynamic light scattering and ζ-potential measurements were conducted on the Nano-ZS instrument (Malvern Instruments Limited). The UV–vis–NIR absorption spectra were acquired on the 5000 UV–vis–NIR spectrophotometer. Fourier transform infrared spectroscopy was performed on a FT-IR spectrometer (Equinox 55, Bruker) in the wavelength range between 4000 and 500 cm^{-1}. *In vivo* photoacoustic imaging was conducted on a PA system (Endra Nexus 128, USA), and the T_2-weighted MR images were obtained on the a 1.5 T Signa HDxt superconductor clinical MR system (GE Medical, Milwaukee, WI).

Preparation of Targeting Substances. Two milliliters of CS (0.8 mg/mL) and 2 mL of SMP (2 mg/mL) were mixed and stirred 12 h for activation before 50 mg of ACPP was added . After being stirred at room temperature overnight, CS-ACPP was obtained by removing unreactive substances by dialysis for 12 h. The NHS and EDC were mixed with 2 mL of RGD (10 mg/mL) and activated for 2 h. After 2 mL of CS (0.8 mg/mL) was added and reacted overnight, dialysis was performed to remove the unreacted substances to obtain the target substance CS-RGD.

Preparation of CS-Decorated Se NPs (Se NCs). Three hundred microliters of Na_2SeO_3 (100 mM) was added gradually to 1.2 mL of Vc (100 mM). After 15 min, 0.6 mL of CS (0.8 mg/mL) was added to a Milli-Q set volume of 10 mL and reacted overnight. Afterward, dialysis was performed to remove unreacted materials.

Preparation of Au NRs. Au NRs were prepared as previously reported method in the literature.[31]

Preparation of Au@Se NCs. Two milliliters of the Au NR (0.1 mg/mL) solution was mixed with 1.2 mL of Vc (100 mM), and 300 μL of Na_2SeO_3 (100 mM) was added gradually. After 15 min, 0.6 mL of CS (0.8 mg/mL) was added to a Milli-Q set volume of 10 mL and reacted overnight. Afterward, dialysis was performed to remove the unreacted materials.

Preparation of Au@Se-R NCs. Two milliliters of the Au NR (0.1 mg/mL) solution was mixed with 1.2 mL of Vc (100 mM), and 300 μL of Na_2SeO_3 (100 mM) was added gradually. After 15 min, 0.6 mL of the CS (0.8 mg/mL) solution and 0.4 mL of CS-RGD were added to a Milli-Q set volume of 10 mL and reacted overnight. Afterward, dialysis was performed to remove the unreacted materials.

Preparation of Au@Se-A NCs. Two milliliters of the Au NR (0.1 mg/mL) solution was mixed with 1.2 mL of Vc (100 mM), and 300 μL of Na_2SeO_3 (100 mM) was added gradually. After 15 min, 0.6 mL of the CS (0.8 mg/mL) solution and 0.4 mL of CS-ACPP were added to a Milli-Q set volume of 10 mL and reacted overnight. Afterward, dialysis was performed to remove the unreacted materials.

Preparation of Au@Se-R/A NCs. Two milliliters of the Au NR (0.1 mg/mL) solution was mixed with 1.2 mL of Vc (100 mM), and 300 μL of Na_2SeO_3 (100 mM) was added gradually. After 15 min, 0.6 mL of the CS (0.8 mg/mL) solution, 0.4 mL CS-ACPP, and 0.4 mL CS-RGD were added to a Milli-Q set volume of 10 mL and reacted overnight. Afterward, dialysis was performed to remove the unreacted materials.

Preparation of Coumarin-6-Loaded Au@Se NCs and Au@Se-R/A NCs. To form coumarin-6-loaded Au@Se NCs and Au@Se-R/A NCs, the remaining steps remain unchanged except a fluorescein coumarin-6 at a final concentration of 5 μg/mL was mixed with Vc and Au NR solution.

Determination of the Content of NC-Grafted Target Material. The Au@Se-R NCs and Au@Se-A NCs were removed from the reaction solution by centrifugation. The supernatant was collected, and the residual peptides were determined by a BCA assay kit. The conjugated content of each peptide (μg/mg NCs) was calculated by the difference value compared with the amount added.

Stability Analysis. Two hundred microliters of the suspensions of various nanoparticles was dispersed in three media including water, 800 μL of 10% FBS in DEM, and 800 μL of serum. The change in the particle size was determined on a Nano-ZS instrument at different time points, and the samples were preserved in a 4 °C refrigerator.

Cell Culture and MTT Assays. The human melanoma A375 cells and L02 were purchased from American Type Culture Collection (ATCC, Manassas, VA, USA). The cells were maintained in the DMEM medium supplemented with 10% fetal bovine serum, 100 units/mL penicillin, and 50 units/mL streptomycin at 37 °C in CO_2 incubator (95% relative humidity, 5% CO_2). The cell viability with and without X-ray irradiation was determined by measuring with MTT.[53]

Cellular Uptake of Au@Se NCs and Au@Se-R/A NCs. The uptake of Au@Se NCs and Au@Se-R/A NCs by A375 cells and L02 cells was quantified as previously described.[25] A fluorescence microplate reader (SpectraMax M5, MD, USA) was employed to measure the fluorescence intensity of coumarin-6 with excitation and emission wavelengths set at 466 and 504 nm, respectively. The cellular uptake efficiency was expressed as the percentage of nanoparticles adsorbed over that added.

Isobologram Analysis. The synergistic effect between X-ray and Au@Se-R/A NCs was examined by isobologram analysis. Briefly, a curve was plotted with the IC_{50} values of Au@Se-R/A NCs and X-ray as the *X*- and *Y*-axes, respectively. The point in the isobologram represents the concentration of X-ray and Au@Se-R/A NCs at the IC_{50} value of the combined treatment. If the data point falls on the straight line, the interaction between X-ray and Au@Se-R/A NCs is an additive effect, but if the point lies above or below the straight line, it represents antagonism or synergism effect, respectively.

Drug Treatment and Radiation. The cells were initially cultured for 24 h and cultured with various doses of nanoparticles for 6 h. Afterward, the cells were irradiated by X-ray (4 Gy) followed by incubation at 37.8 °C for 72 h.

Flow Cytometric Analysis. The cell cycle distribution and cell apoptosis after the treatment of nanoparticles and X-ray were analyzed by flow cytometric analysis as previously reported.[54]

Measurement of Intracellular Reactive Oxygen Species Generation. The effects of the nanoparticles on intracellular ROS generation in the cell-free and cell models were examined by DCF fluorescence assay.[25] In the cell model and cell-free model, A375 cells

DOI: 10.1021/acsnano.7b01346
ACS Nano 2017, 11, 4848–4858

at a density of 5×10^5 cells/mL were incubated with nanoparticles for 6 h. The cells with or without X-ray (4 Gy) were treated with the DCF probe at a final concentration of 32 μM. Intracellular ROS generation was detected as the fluorescence intensity of DCF. The cell-free model consisted of that described above except that the seeded A375 cells were replaced with the PBS solution.

Western Blot Analysis. The total cellular proteins (1×10^5 cells/mL, 10 mL) treated with or without nanoparticles and X-ray were extracted by cell lysis buffer from Cell Signaling Technology. The protein concentrations were measured by BCA protein assay, and the effects of nanoparticles and X-ray on the expression levels of the related proteins were determined by Western blotting.

A375 MCTS. The A375 cells (2×10^5 cells/well) were seeded on an ultralow adsorption 6-well plate, which was agitated gently in a shock incubator for 5 days.

Penetrating Ability into A375 Spheroids. The A375 MCTS were treated with the coumarin-6-loaded nanoparticles, Au@Se NCs and Au@Se-R/A NCs for 8 h. The MCTS were scanned from the different layers from the top of the spheroid to the middle using a confocal laser scanning fluorescent microscope (Zeiss LSM 700).

Inhibitory Effect. The size of MCTS was used to estimate the inhibitory effect. A375 MCTS were incubated with Au@Se NCs and Au@Se-A/R NCs for 8 h, and the tumor volume was measured by an inverted microscope at days 0, 1, 2, 3, and 4. The major (d_{max}) and minor (d_{min}) diameters of each spheroid were determined, and the spheroid volume was calculated by the following formula: $V = (\pi \times d_{max} \times d_{min})/6$. The volume change ratio of A375 MCTS was calculated by the formula $R = (V_{day}\ i/V_{day}\ 0) \times 100\%$. Each assay was repeated in triplicate, and sextuplicate determinations were set for each dose level.

Preparation of Subcutaneous Nude Mouse Models with A375 Cancer Cells. The animal experiments were carried out in the Animal Experimentation Ethics Committee of Jinan University. Briefly, about 1×10^6 A375 human melanoma tumor cells in 100 μL of the serum-free medium were subcutaneously injected into the right back of male nude mice. After the tumor grew to approximately 5 mm, follow-up tests were performed.

Radiotherapy Treatment. Conventional fractionation and single large dose radiotherapy were adopted using a digital high-energy linear accelerator, 6 MV electron beam, X-ray tumor local radiation, source to skin distance of 100 cm, 1 times/2 day, 4 Gy/times, and total dose of 40 Gy.

Therapeutic Effects in Mouse Models with A375 Human Melanoma Tumor. The tumor-bearing mice were randomly divided into six groups. The first group was IV injected with 125 μL of saline as the control group; the second group was treated with X-ray (4 Gy); the third group was IV injected with 125 μL of Au@Se-R/A dispersion (2.0 mg/kg, the concentration of Se) every other day; the fourth group was IT injected with 125 μL of Au@Se-R/A dispersion (2.0 mg/kg, the concentration of Se) every other day; the fifth group was IV injected with 125 μL of Au@Se-R/A dispersion (2.0 mg/kg, the concentration of Se) every other day and after 6 h exposed to X-ray (4 Gy); the sixth group was IT injected with 125 μL of Au@Se-R/A dispersion (2.0 mg/kg, the concentration of Se) every other day and immediately exposed to X-ray (4 Gy). After 21 days, the tumors were harvested, weighed, fixed with formalin, embedded with paraffin, and sectioned. X-ray irradiation was performed immediately after injection with the Au@Se-R/A NP dispersion. The therapeutic X-ray irradiation was applied at 6 h postinjection (IV) with either NCs or saline.

***In Vivo* Photoacoustic Imaging of A375 Tumor Models.** *In vivo* photoacoustic imaging was implemented on a photoacoustic system with the excitation laser set at 800 nm. The mice were injected intraperitoneally with 2% pentobarbital before the experiment. Nude mice with A375 xenograft subcutaneous models were IV injected with 2 mg/kg Au@Se-R/A NCs, and the photoacoustic signal of nanoparticles was detected at 2, 4, and 6 h.

MRI Acquisition. The MR images were obtained on a 3.0-TMR scanner (General Electric, Milwaukee, WI, USA), and the T_2-weighted images (T_2 WI) of the nude mice with A375 xenograft subcutaneous models were obatined 21 days after the different treatments.

Acute Toxicity Experiments. In order to determine the side effects of the X-ray and Au@Se-R/A NC treatments on vital organs, the mice in different groups were sacrificed after 21 days. The important organs such as the heart, liver, spleen, lung, and kidney were acquired, fixed with formalin, embedded with paraffin, and sectioned. Blood samples were also collected and analyzed.

Biodistribution Studies. The concentrations of Au and Se in the tumor and other organs were determined. The biodistributions of the functionalized Au@Se-R/A NCs in tissues associated with clearance (liver, spleen, and kidney) as well as the gastric tumor, lung, and heart were measured by inductively coupled plasma mass spectrometry.

Statistics Analysis. All the experiments were carried out in triplicate and the data expressed as mean ± standard deviation. The differences between the control and experimental groups were analyzed by the two-tailed Student's t test. One-way analysis of variance was used in multiple group comparisons, and statistical analysis was performed using SPSS statistical program version 13 (SPSS Inc., Chicago, IL). Significant differences between the treatment and control groups are indicated at $^*P < 0.05$.

ASSOCIATED CONTENT

Supporting Information

The Supporting Information is available free of charge on the ACS Publications website at DOI: 10.1021/acsnano.7b01346.

Stability of different nanosystems (Figure S1); A375 cells under X-ray (0−8 Gy) irradiation and then incubated for another 72 h (Figure S2); high-magnification TEM image of Au@Se-R/A NCs after X-ray irradiation (4 Gy) (Figure S3); Au@Se-R/A NCs synergistically enhances the anticancer efficacy compared to that of the free Se NCs and Au NPs (Figure S4); cumulative uptake of Au@Se-R/A NCs nanoparticles by A375 cells for different time periods (Figure S5); flow cytometric analysis of A375 cells after treatment of Au NRs, Se NCs, Au@Se NCs, and with or without X-ray showing enhanced apoptosis in A375 cells (Figure S6); activation of apoptotic pathways (Figure S7); different nanosystems enhance radiation-induced ROS generation (Figure S8); optoacoustic signals of tumor sites at different time after intravenous injection of Au@Se-R/A NCs (2 mg/kg) (Figure S9); changes in body weight for different groups of tumor-bearing mice (21 days) (Figure S10); growth inhibition of different NP or NC radiation treatment on A375 (calculated by Se concentration, 72 h) (Table S1); growth inhibition of different NP or NC radiation treatment on A375 (calculated by Au concentration, 72 h) (Table S2); cytotoxicity of Au NRs, Se NCs, Au@Se NCs, and Au@Se-R/A NCs without X-ray treatment to L02 cells (72 h) (Table S3) (PDF)

AUTHOR INFORMATION

Corresponding Authors

*E-mail: xf.yu@siat.ac.cn.
*E-mail: tchentf@jnu.edu.cn.

ORCID

Xue-Feng Yu: 0000-0003-2566-6194
Tianfeng Chen: 0000-0001-6953-1342

Notes

The authors declare no competing financial interest.

ACKNOWLEDGMENTS

This work was supported by Science Foundation for Distinguished Young Scholars of Guangdong Province

DOI: 10.1021/acsnano.7b01346
ACS Nano 2017, 11, 4848−4858

(2013050014667), Natural Science Foundation of China (21371076), National High-level personnel of special support program (2014189), YangFan Innovative & Entepreneurial Research Team Project (201312H05), Guangdong Special Support Program and Guangdong Frontier Key Technological Innovation Special Funds (2014B050505012), Fundamental Research Funds for the Central Universities, and Hong Kong Research Grants Council (RGC) General Research Funds (GRF) No. City U11301215.

REFERENCES

(1) Wang, S. G.; Li, X.; Chen, Y.; Cai, X. J.; Yao, H. L.; Gao, W.; Zheng, Y. Y.; An, X.; Shi, J. L.; Chen, H. R. A Facile One-Pot Synthesis of a Two-Dimensional MoS_2/Bi_2S_3 Composite Theranostic Nanosystem for Multi-Modality Tumor Imaging and Therapy. *Adv. Mater.* **2015**, *27*, 2775−2782.

(2) Song, G. S.; Liang, C.; Gong, H.; Li, M. F.; Zheng, X. C.; Cheng, L.; Yang, K.; Jiang, X. Q.; Liu, Z. Core-Shell MnSe@Bi_2Se_3 Fabricated *Via* a Cation Exchange Method as Novel Nanotheranostics for Multimodal Imaging and Synergistic Thermoradiotherapy. *Adv. Mater.* **2015**, *27*, 6110−6117.

(3) Song, G. S.; Chen, Y. Y.; Liang, C.; Yi, X.; Liu, J. J.; Sun, X. Q.; Shen, S. D.; Yang, K.; Liu, Z. Catalase-Loaded TaOx Nanoshells as Bio-Nanoreactors Combining High-Z Element and Enzyme Delivery for Enhancing Radiotherapy. *Adv. Mater.* **2016**, *28*, 7143−7148.

(4) Fan, W. P.; Shen, B.; Bu, W. B.; Chen, F.; Zhao, K. L.; Zhang, S. J.; Zhou, L. P.; Peng, W. J.; Xiao, Q. F.; Xing, H. Y.; Liu, J. N.; Ni, D. L.; He, Q. J.; Shi, J. L. Rattle-Structured Multifunctional Nanotheranostics for Synergetic Chemo-/Radiotherapy and Simultaneous Magnetic/Luminescent Dual-Mode Imaging. *J. Am. Chem. Soc.* **2013**, *135*, 6494−6503.

(5) Deng, Z. Q.; Yu, L. L.; Cao, W. Q.; Zheng, W. J.; Chen, T. F. A Selenium-Containing Ruthenium Complex as a Cancer Radiosensitizer, Rational Design and the Important Role of ROS-Mediated Signalling. *Chem. Commun.* **2015**, *51*, 2637−2640.

(6) Xie, Q.; Lan, G. Q.; Zhou, Y. L.; Huang, J. M.; Liang, Y. W.; Zheng, W. J.; Fu, X. Y.; Fan, C. D.; Chen, T. F. Strategy to Enhance the Anticancer Efficacy of X-ray Radiotherapy in Melanoma Cells by Platinum Complexes, the Role of ROS-Mediated Signaling Pathways. *Cancer Lett.* **2014**, *354*, 58−67.

(7) Fan, W. P.; Bu, W. B.; Shen, B.; He, Q. J.; Cui, Z. W.; Liu, Y. Y.; Zheng, X. P.; Zhao, K. L.; Shi, J. L. Intelligent MnO_2 Nanosheets Anchored with Upconversion Nanoprobes for Concurrent PH-/H_2O_2-Responsive UCL Imaging and Oxygen-Elevated Synergetic Therapy. *Adv. Mater.* **2015**, *27*, 4155−4161.

(8) Chen, Q.; Feng, L. Z.; Liu, J. J.; Zhu, W. W.; Dong, Z. L.; Wu, Y. F.; Liu, Z. Intelligent Albumin-MnO_2 Nanoparticles as PH-/H_2O_2-Responsive Dissociable Nanocarriers to Modulate Tumor Hypoxia for Effective Combination Therapy. *Adv. Mater.* **2016**, *28*, 7129−7136.

(9) Zhong, X. Y.; Yang, K.; Dong, Z. L.; Yi, X.; Wang, Y.; Ge, C. C.; Zhao, Y. L.; Liu, Z. Polydopamine as a Biocompatible Multifunctional Nanocarrier for Combined Radioisotope Therapy and Chemotherapy of Cancer. *Adv. Funct. Mater.* **2015**, *25*, 7327−7336.

(10) Cheng, L.; Shen, S. D.; Shi, S. X.; Yi, Y.; Wang, X. Y.; Song, G. S.; Yang, K.; Liu, G.; Barnhart, T. E.; Cai, W. B.; Liu, Z. $FeSe_2$-Decorated Bi_2Se_3 Nanosheets Fabricated *Via* Cation Exchange for Chelator-Free Cu-64-Labeling and Multimodal Image-Guided Photothermal-Radiation Therapy. *Adv. Funct. Mater.* **2016**, *26*, 2185−2197.

(11) Song, G. S.; Liang, C.; Yi, X.; Zhao, Q.; Cheng, L.; Yang, K.; Liu, Z. A. Perfluorocarbon-Loaded Hollow Bi_2Se_3 Nanoparticles for Timely Supply of Oxygen under Near-Infrared Light to Enhance the Radiotherapy of Cancer. *Adv. Mater.* **2016**, *28*, 2716−2723.

(12) Zhang, X. D.; Chen, J.; Min, Y.; Park, G. B.; Shen, X.; Song, S. S.; Sun, Y. M.; Wang, H.; Long, W.; Xie, J. P.; Gao, K.; Zhang, L. F.; Fan, S. J.; Fan, F. Y.; Jeong, U. Metabolizable Bi_2Se_3 Nanoplates: Biodistribution, Toxicity, and Uses for Cancer Radiation Therapy and Imaging. *Adv. Funct. Mater.* **2014**, *24*, 1718−1729.

(13) Chetty, I. J.; Martel, M. K.; Jaffray, D. A.; Benedict, S. H.; Hahn, S. M.; Berbeco, R.; Deye, J.; Jeraj, R.; Kavanagh, B.; Krishnan, S.; Lee, N.; Low, D. A.; Mankoff, D.; Marks, L. B.; Ollendorf, D.; Paganetti, H.; Ross, B.; Siochi, R. A. C.; Timmerman, R. D.; Wong, J. W. Technology for Innovation in Radiation Oncology. *Int. J. Radiat. Oncol., Biol., Phys.* **2015**, *93*, 485−492.

(14) Hainfeld, J. F.; Slatkin, D. N.; Smilowitz, H. M. The Use of Gold Nanoparticles to Enhance Radiotherapy in Mice. *Phys. Med. Biol.* **2004**, *49*, N309−N315.

(15) Hainfeld, J. F.; Dilmanian, F. A.; Slatkin, D. N.; Smilowitz, H. M. Radiotherapy Enhancement with Gold Nanoparticles. *J. Pharm. Pharmacol.* **2008**, *60*, 977−985.

(16) Misawa, M.; Takahashi, J. Generation of Reactive Oxygen Species Induced by Gold Nanoparticles under X-ray and UV Irradiations. *Nanomedicine* **2011**, *7*, 604−614.

(17) Zhang, X. D.; Luo, Z. T.; Chen, J.; Shen, X.; Song, S. S.; Sun, Y. M.; Fan, S. J.; Fan, F. Y.; Leong, D. T.; Xie, J. P. Ultrasmall $Au_{10-12}(SG)_{(10-12)}$ Nanomolecules for High Tumor Specificity and Cancer Radiotherapy. *Adv. Mater.* **2014**, *26*, 4565−4568.

(18) Chen, W.; Zhang, S.; Yu, Y.; Zhang, H.; He, Q. Structural-Engineering Rationales of Gold Nanoparticles for Cancer Theranostics. *Adv. Mater.* **2016**, *28*, 8567−8585.

(19) Ke, H. T.; Yue, X. L.; Wang, J. R.; Xing, S.; Zhang, Q.; Dai, Z. F.; Tian, J.; Wang, S. M.; Jin, Y. S. Gold Nanoshelled Liquid Perfluorocarbon Nanocapsules for Combined Dual Modal Ultrasound/CT Imaging and Photothermal Therapy of Cancer. *Small* **2014**, *10*, 1220−1227.

(20) Li, Z. B.; Huang, H.; Tang, S. Y.; Li, Y.; Yu, X. F.; Wang, H. Y.; Li, P. H.; Sun, Z. B.; Zhang, H.; Liu, C. L.; Chu, P. K. Small Gold Nanorods Laden Macrophages for Enhanced Tumor Coverage in Photothermal Therapy. *Biomaterials* **2016**, *74*, 144−154.

(21) Shi, P.; Liu, Z.; Dong, K.; Ju, E. G.; Ren, J. S.; Du, Y. D.; Li, Z. Q.; Qu, X. G. A Smart "Sense-Act-Treat" System: Combining a Ratiometric PH Sensor with a near Infrared Therapeutic Gold Nanocage. *Adv. Mater.* **2014**, *26*, 6635−6641.

(22) Wang, S. J.; Huang, P.; Nie, L. M.; Xing, R. J.; Liu, D. B.; Wang, Z.; Lin, J.; Chen, S. H.; Niu, G.; Lu, G. M.; Chen, X. Y. Single Continuous Wave Laser Induced Photodynamic/Plasmonic Photothermal Therapy Using Photosensitizer-Functionalized Gold Nanostars. *Adv. Mater.* **2013**, *25*, 3055−3061.

(23) Zheng, T.; Li, G. G.; Zhou, F.; Wu, R.; Zhu, J. J.; Wang, H. Gold-Nanosponge-Based Multistimuli-Responsive Drug Vehicles for Targeted Chemo-Photothermal Therapy. *Adv. Mater.* **2016**, *28*, 8218−8226.

(24) Song, J. B.; Yang, X. Y.; Jacobson, O.; Huang, P.; Sun, X. L.; Lin, L. S.; Yan, X. F.; Niu, G.; Ma, Q. J.; Chen, X. Ultrasmall Gold Nanorod Vesicles with Enhanced Tumor Accumulation and Fast Excretion from the Body for Cancer Therapy. *Adv. Mater.* **2015**, *27*, 4910−4917.

(25) Huang, Y. Y.; He, L. Z.; Liu, W.; Fan, C. D.; Zheng, W. J.; Wong, Y. S.; Chen, T. F. Selective Cellular Uptake and Induction of Apoptosis of Cancer-Targeted Selenium Nanoparticles. *Biomaterials* **2013**, *34*, 7106−7116.

(26) Liu, W.; Li, X. L.; Wong, Y. S.; Zheng, W. J.; Zhang, Y. B.; Cao, W. Q.; Chen, T. F. Selenium Nanoparticles as a Carrier of 5-Fluorouracil to Achieve Anticancer Synergism. *ACS Nano* **2012**, *6*, 6578−6591.

(27) Jiang, W. T.; Fu, Y. T.; Yang, F.; Yang, Y. F.; Liu, T.; Zheng, W. J.; Zeng, L. L.; Chen, T. F. Gracilaria Iemaneiformis Polysaccharide as Integrin-Targeting Surface Decorator of Selenium Nanoparticles to Achieve Enhanced Anticancer Efficacy. *ACS Appl. Mater. Interfaces* **2014**, *6*, 13738−13748.

(28) Yu, B.; Zhang, Y. B.; Zheng, W. J.; Fan, C. D.; Chen, T. F. Positive Surface Charge Enhances Selective Cellular Uptake and Anticancer Efficacy of Selenium Nanoparticles. *Inorg. Chem.* **2012**, *51*, 8956−8963.

(29) Liu, T.; Lai, L.; Song, Z.; Chen, T. Drug Delivery: A Sequentially Triggered Nanosystem for Precise Drug Delivery and Simultaneous Inhibition of Cancer Growth, Migration, and Invasion. *Adv. Funct. Mater.* **2016**, *26*, 7943−7943.

DOI: 10.1021/acsnano.7b01346
ACS Nano 2017, 11, 4848−4858

(30) Wang, B. K.; Yu, X. F.; Wang, J. H.; Li, Z. B.; Li, P. H.; Wang, H. Y.; Song, L.; Chu, P. K.; Li, C. Z. Gold-Nanorods-Sirna Nanoplex for Improved Photothermal Therapy by Gene Silencing. *Biomaterials* **2016**, *78*, 27−39.
(31) Li, M.; Yu, X. F.; Liang, S.; Peng, X. N.; Yang, Z. J.; Wang, Y. L.; Wang, Q. Q. Synthesis of Au-CdS Core-Shell Hetero-Nanorods with Efficient Exciton-Plasmon Interactions. *Adv. Funct. Mater.* **2011**, *21*, 1788−1794.
(32) Hu, J. J.; Xiao, D.; Zhang, X. Z. Advances in Peptide Functionalization on Mesoporous Silica Nanoparticles for Controlled Drug Release. *Small* **2016**, *12*, 3344−3359.
(33) He, L. Z.; Huang, Y. Y.; Zhu, H. L.; Pang, G. H.; Zheng, W. J.; Wong, Y. S.; Chen, T. F. Cancer-Targeted Monodisperse Mesoporous Silica Nanoparticles as Carrier of Ruthenium Polypyridyl Complexes to Enhance Theranostic Effects. *Adv. Funct. Mater.* **2014**, *24*, 2754−2763.
(34) Cheng, H.; Zhu, J. Y.; Xu, X. D.; Qiu, W. X.; Lei, Q.; Han, K.; Cheng, Y. J.; Zhang, X. Z. Activable Cell-Penetrating Peptide Conjugated Prodrug for Tumor Targeted Drug Delivery. *ACS Appl. Mater. Interfaces* **2015**, *7*, 16061−16069.
(35) Liu, Z.; Xiong, M.; Gong, J. B.; Zhang, Y.; Bai, N.; Luo, Y. P.; Li, L. Y.; Wei, Y. Q.; Liu, Y. H.; Tan, X. Y.; Xiang, R. Legumain Protease-Activated TAT-Liposome Cargo for Targeting Tumours and Their Microenvironment. *Nat. Commun.* **2014**, *5*, 4280−4290.
(36) Sun, Z. H.; Yang, Z.; Zhou, J. H.; Yeung, M. H.; Ni, W. H.; Wu, H. K.; Wang, J. F. A General Approach to the Synthesis of Gold-Metal Sulfide Core-Shell and Heterostructures. *Angew. Chem., Int. Ed.* **2009**, *48*, 2881−2885.
(37) He, L. Z.; Ji, S. B.; Lai, H. Q.; Chen, T. F. Selenadiazole Derivatives as Theranostic Agents for Simultaneous Cancer Chemo-/Radiotherapy by Targeting Thioredoxin Reductase. *J. Mater. Chem. B* **2015**, *3*, 8383−8393.
(38) Beskow, C.; Skikuniene, J.; Holgersson, A.; Nilsson, B.; Lewensohn, R.; Kanter, L.; Viktorsson, K. Radioresistant Cervical Cancer Shows Upregulation of the NHEJ Proteins DNA-PKcs, Ku70 and Ku86. *Br. J. Cancer* **2009**, *101*, 816−821.
(39) Wang, M.; Morsbach, F.; Sander, D.; Gheorghiu, L.; Nanda, A.; Benes, C.; Kriegs, M.; Krause, M.; Dikomey, E.; Baumann, M.; Dahm-Daphi, J.; Settleman, J.; Willers, H. Willers, H. EGF Receptor Inhibition Radiosensitizes NSCLC Cells by Inducing Senescence in Cells Sustaining DNA Double-Strand Breaks. *Cancer Res.* **2011**, *71*, 6261−6269.
(40) Valcarcel, M.; Carrascal, T.; Crende, O.; Vidal-Vanaclocha, F. IL-18 Regulates Melanoma VLA-4 Integrin Activation through a Hierarchized Sequence of Inflammatory Factors. *J. Invest. Dermatol.* **2014**, *134*, 470−480.
(41) Ryschich, E.; Huszty, G.; Knaebel, H. P.; Hartel, M.; Buchler, M. W.; Schmidt, J. Transferrin Receptor Is a Marker of Malignant Phenotype in Human Pancreatic Cancer and in Neuroendocrine Carcinoma of the Pancreas. *Eur. J. Cancer* **2004**, *40*, 1418−1422.
(42) Li, S. Y.; Cheng, H.; Qiu, W. X.; Liu, L. H.; Chen, S.; Hu, Y.; Xie, B. R.; Li, B.; Zhang, X. Z. Protease-Activable Cell-Penetrating Peptide-Protoporphyrin Conjugate for Targeted Photodynamic Therapy. *ACS Appl. Mater. Interfaces* **2015**, *7*, 28319−28329.
(43) Olson, E. S.; Aguilera, T. A.; Jiang, T.; Ellies, L. G.; Nguyen, Q. T.; Wong, E. H.; Gross, L. A.; Tsien, R. Y. *In Vivo* Characterization of Activatable Cell Penetrating Peptides for Targeting Protease Activity in Cancer. *Integr. Biol.* **2009**, *1*, 382−393.
(44) Huang, S. X.; Shao, K.; Liu, Y.; Kuang, Y. Y.; Li, J. F.; An, S.; Guo, Y. B.; Ma, H. J.; Jiang, C. Tumor-Targeting and Microenvironment-Responsive Smart Nanoparticles for Combination Therapy of Antiangiogenesis and Apoptosis. *ACS Nano* **2013**, *7*, 2860−2871.
(45) He, L. Z.; Lai, H. Q.; Chen, T. F. Dual-Function Nanosystem for Synergetic Cancer Chemo-/Radiotherapy through ROS-Mediated Signaling Pathways. *Biomaterials* **2015**, *51*, 30−42.
(46) Huang, H. Y.; Yu, B. L.; Zhang, P. Y.; Huang, J. J.; Chen, Y.; Gasser, G.; Ji, L. N.; Chao, H. Highly Charged Ruthenium(II) Polypyridyl Complexes as Lysosome-Localized Photosensitizers for Two-Photon Photodynamic Therapy. *Angew. Chem., Int. Ed.* **2015**, *54*, 14049−14052.
(47) You, Y. Y.; Hu, H.; He, L. Z.; Chen, T. F. Differential Effects of Polymer-Surface Decoration on Drug Delivery, Cellular Retention, and Action Mechanisms of Functionalized Mesoporous Silica Nanoparticles. *Chem. - Asian J.* **2015**, *10*, 2541.
(48) Chen, Q.; Feng, L.; Liu, J.; Zhu, W.; Dong, Z.; Wu, Y.; Liu, Z. Intelligent Albumin-MnO_2 Nanoparticles as PH-/H_2O_2-Responsive Dissociable Nanocarriers to Modulate Tumor Hypoxia for Effective Combination Therapy. *Adv. Mater.* **2016**, *28*, 7129−7136.
(49) Huang, Y. Y.; Luo, Y.; Zheng, W. J.; Chen, T. F. Rational Design of Cancer-Targeted BSA Protein Nanoparticles as Radiosensitizer to Overcome Cancer Radioresistance. *ACS Appl. Mater. Interfaces* **2014**, *6*, 19217−19228.
(50) Wang, N.; Feng, Y. X.; Zeng, L. L.; Zhao, Z. N.; Chen, T. F. Functionalized Multiwalled Carbon Nanotubes as Carriers of Ruthenium Complexes to Antagonize Cancer Multidrug Resistance and Radioresistance. *ACS Appl. Mater. Interfaces* **2015**, *7*, 14933−14945.
(51) Dixon, A. J.; Hu, S.; Klibanov, A. L.; Hossack, J. A. Oscillatory Dynamics and *In Vivo* Photoacoustic Imaging Performance of Plasmonic Nanoparticle-Coated Microbubbles. *Small* **2015**, *11*, 3066−3077.
(52) Song, J. B.; Yang, X. Y.; Jacobson, O.; Lin, L. S.; Huang, P.; Niu, G.; Ma, Q. J.; Chen, X. Y. Sequential Drug Release and Enhanced Photothermal and Photoacoustic Effect of Hybrid Reduced Graphene Oxide-Loaded Ultrasmall Gold Nanorod Vesicles for Cancer Therapy. *ACS Nano* **2015**, *9*, 9199−9209.
(53) Chen, T. F.; Wong, Y. S. Selenocystine Induces Reactive Oxygen Species-Mediated Apoptosis in Human Cancer Cells. *Biomed. Pharmacother.* **2009**, *63*, 105−113.
(54) Liu, M. X.; Chang, Y. Z.; Yang, J.; You, Y. Y.; He, R.; Chen, T. F.; Zhou, C. R. Functionalized Halloysite Nanotube by Chitosan Grafting for Drug Delivery of Curcumin to Achieve Enhanced Anticancer Efficacy. *J. Mater. Chem. B* **2016**, *4*, 2253−2263.

DOI: 10.1021/acsnano.7b01346
ACS Nano 2017, 11, 4848−4858

Supplementary Information

Designing Core-Shell Gold and Selenium Nanocomposites for Cancer Radiochemotherapy

Yanzhou Chang[1], Lizhen He[1], Zhibin Li[2], Lilan Zeng[1], Zhenhuan Song[1], Penghui Li[2], Leung Chan[2], Yuanyuan You[1], Xue-Feng Yu[2,*], Paul K Chu[3], Tianfeng Chen[1,*]

[1] Department of Chemistry, Jinan University, Guangzhou ,510632 (P. R. China).

[2] Institute of Biomedicine and Biotechnology, Shenzhen Institutes of Advanced Technology, Chinese Academy of Sciences, Shenzhen, 518055 (P. R. China).

[3] Department of Physics and Materials Science, City University of Hong Kong, Tat Chee Avenue, Kowloon, Hong Kong, China.

*To whom correspondence should be addressed. Tel: +86 20-85225962.

*_**Corresponding author**_: Tel: +86 20-85225962.

E-mails: tchentf@jnu.edu.cn (T. Chen), xf.yu@siat.ac.cn (X. F. Yu).

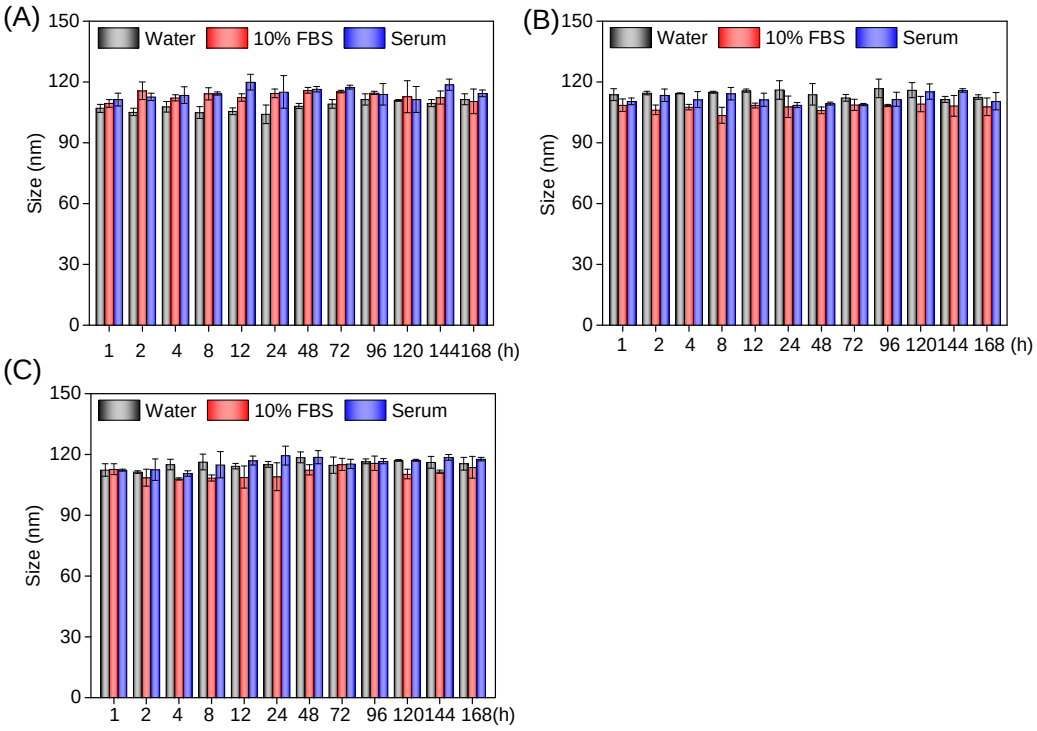

Figure S1. Stability of different nanosystems. (A) Changes in the hydrodynamic size of Au@Se NCs in water, 10% FBS, and human FBS. (B) Changes in the hydrodynamic size of Au@Se-R NCs in water, 10% FBS, and human FBS. (C) Changes in the hydrodynamic size of Au@Se-A NCs in water, 10% FBS, and human FBS. Each value represents means ± SD (n = 3).

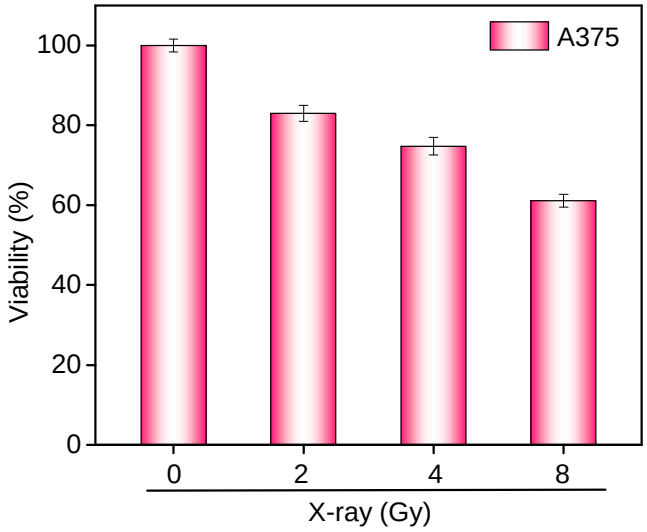

Figure S2. A375 cells under X-ray (0–8 Gy) irradiation and then incubated for another 72 h. Each value represents means ± SD (n = 3).

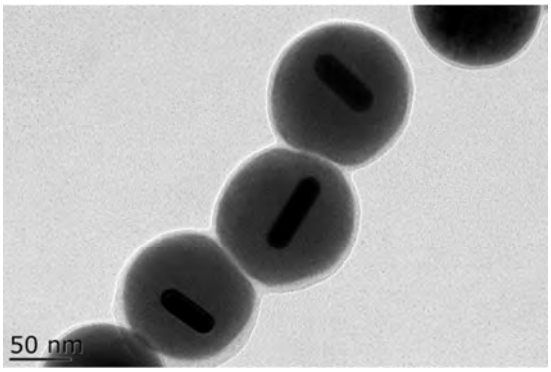

Figure S3. High-magnification TEM image of Au@Se-R/A NCs after X-ray irradiation (4 Gy).

Table S1. Growth inhibition of different NPs or NCs-radiation treatment on A375 (calculated by Se concentration, 72 h).

Sample	IC_{50} (μM)			
	0 Gy	2 Gy	4 Gy	8 Gy
Au NRs	7.72	2.70	2.03	1.53
Se NPs	>64	>64	>64	>64
Se NCs	39.11	24.54	13.44	8.01
Au@Se NCs	21	19.11	6.63	3.86
Au@Se-R NCs	18.78	15.26	5.80	3.08
Au@Se-A NCs	16.27	11.38	5.64	2.69
Au@Se-R/A NCs	10.98	6.81	2.69	1.06

Table S2. Growth inhibition of different NPs or NCs-radiation treatment on A375 (calculated by Au concentration, 72 h).

Sample	IC_{50} (μM)			
	0 Gy	2 Gy	4 Gy	8 Gy
Au@Se NCs	0.49	0.45	0.15	0.09
Au@Se-R NCs	0.43	0.35	0.13	0.07
Au@Se-A NCs	0.44	0.31	0.15	0.07
Au@Se-R/A NCs	0.30	0.19	0.07	0.03

Table S3. Cytotoxicity of Au NRs, Se NCs, Au@Se NCs, Au@Se-R/A NCs without X-ray treatment to L02 cells (72 h).

Sample	IC_{50} (μM)	SI
Au NRs	34.8	4.5
Se NCs	68.1	1.7
Au@Se NCs	50.5	2.4
Au@Se-R/A NCs	53.8	5

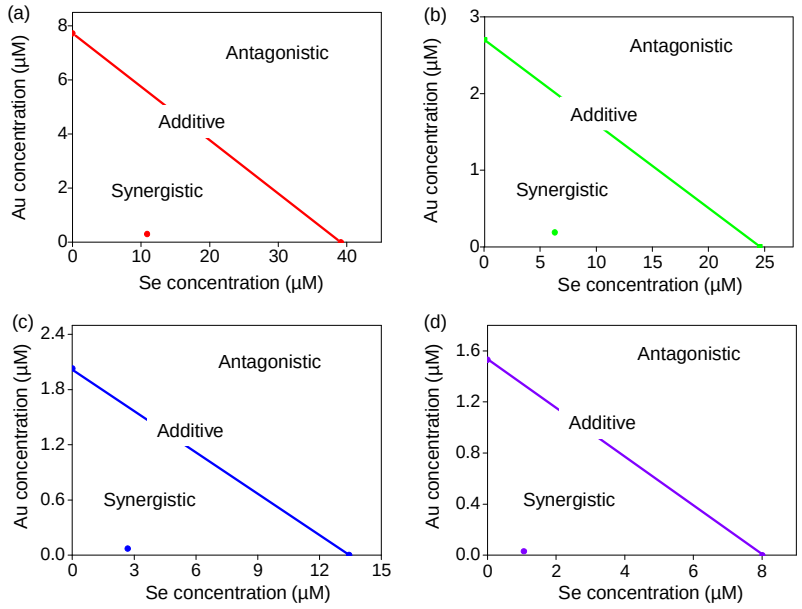

Figure S4. Au@Se-R/A NCs synergistically enhances the anticancer efficacy comparing with the free Se NCs and Au NPs. Isobologram analysis of the synergistic antiproliferative effect co-treated with X-ray and Au@Se -R/A NCs to A375 cells. (A) 0 Gy, (B) 2 Gy, (C) 4 Gy and (D) 8 Gy. The data points in the isobologram correspond to the growth inhibition ratio at 50% in the combined treatment.

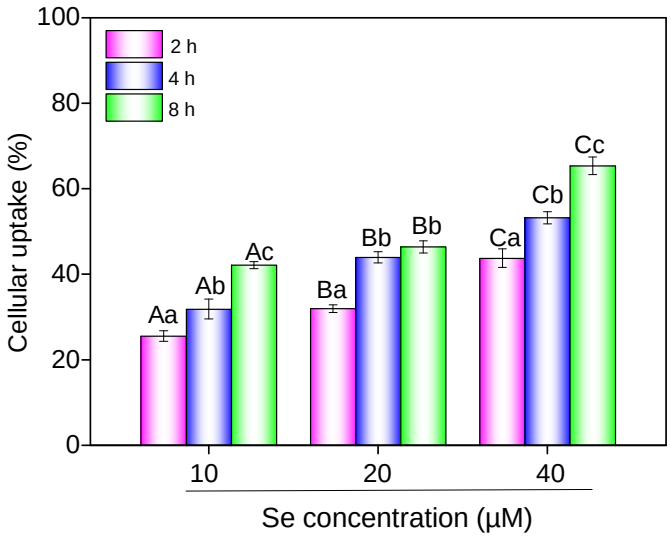

Figure S5. Cumulative uptake of Au@Se-R/A NCs nanoparticles by A375 cells for different time periods. The uptake of Au@Se-R/A NCs increases in a time- and dose-dependent manner. The upper case letters indicate significant differences at the $P < 0.05$ level between groups and lower case letters indicate significant differences at the $P < 0.05$ level within groups. Each value represents means ± SD ($n = 3$).

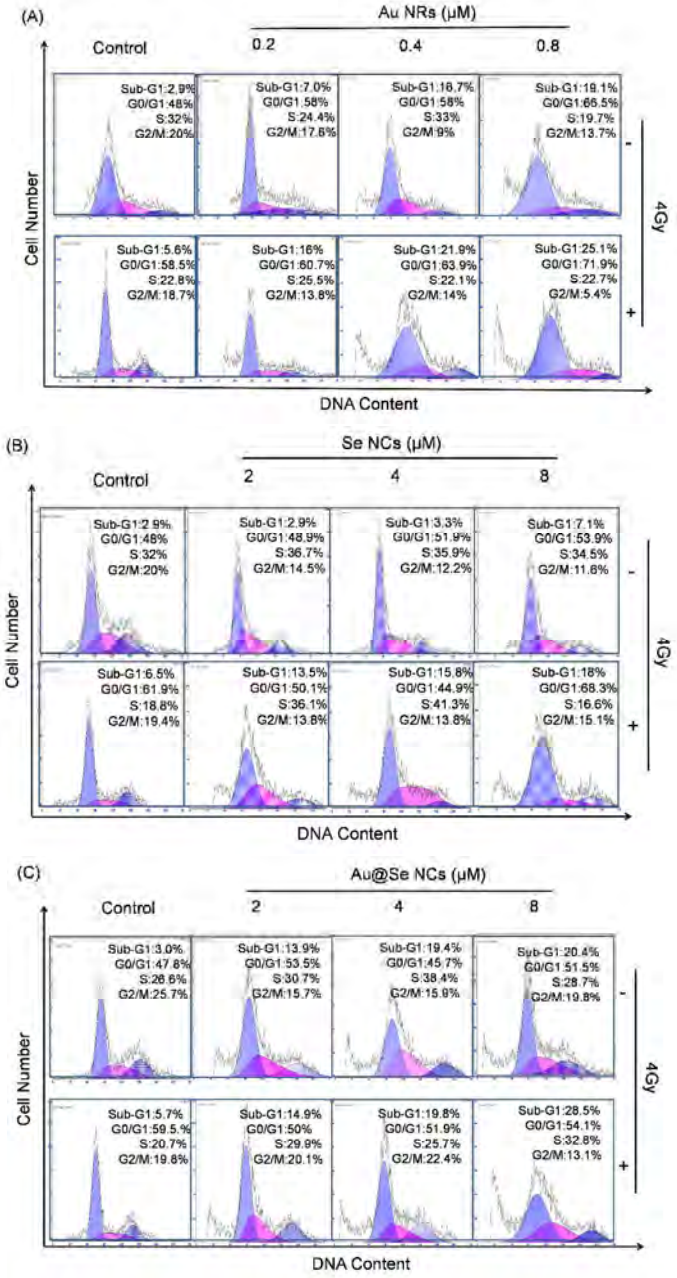

Figure S6. Flow cytometric analysis of A375 cells after treatment of (A) Au NRs, (B) Se NCs, (C) Au@Se NCs and with or without X-ray showing enhanced apoptosis in A375 cells. The cell cycle distribution after different treatments is analyzed by quantifying the DNA content using flow cytometry.

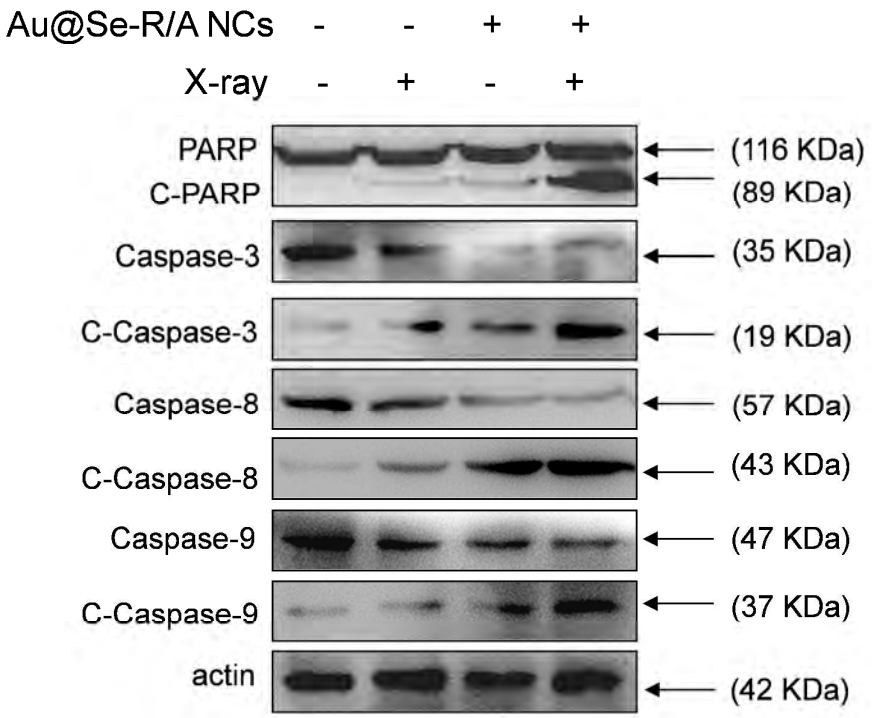

Figure S7. Activation of apoptotic pathways. The cells were treated with the combined treatment of Au@Se-R/A NCs (20 μM) and X-ray (4Gy), and then Western blotting was employed to analyze PARP and caspases cleavage in cell apoptosis induced by Au@Se-R/A NCs with (+) and without (−) X-ray.

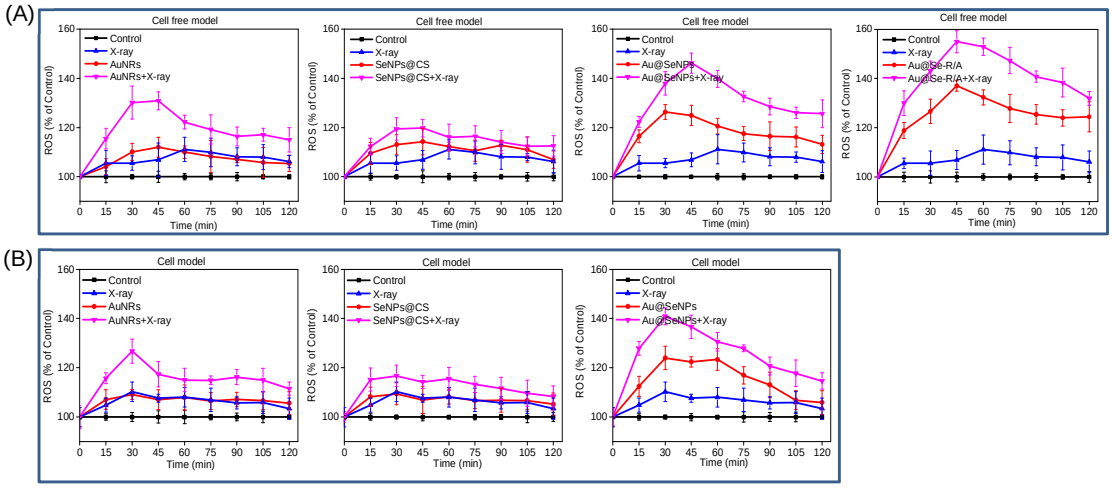

Figure S8. Different nanosystems enhance radiation-induced ROS generation. (A) Effects of Au NRs (0.88 μM), Se NCs (32 μM), Au@Se NCs (32 μM), and Au@Se-R/A NCs (32 μM) with or without X-ray on ROS generation in the cell-0free model. (B) Effects of Au NRs (0.88 μM), Se NCs (32 μM), Au@Se NCs (32 μM), and Au@Se-R/A NCs (32 μM) with or without X-ray on ROS generation in A375 cells. Each value represents means ± SD (n = 3).

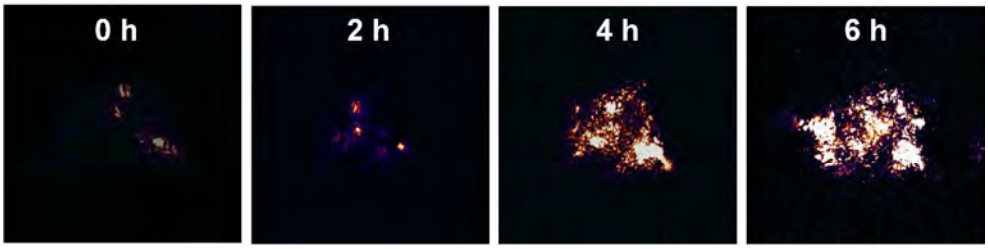

Figure S9. Optoacoustic signals of tumor sites at different time after intravenous injection of Au@Se-R/A NCs (2 mg/kg).

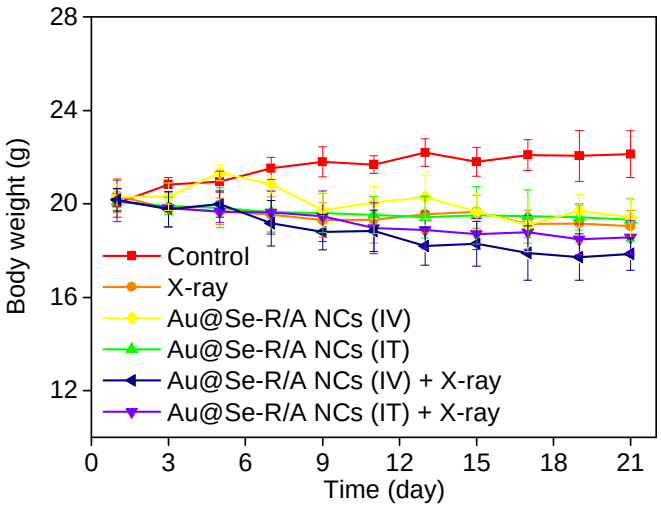

Figure S10. Changes in body weight for different groups of tumor-bearing mice (21 days). Each value represents means ± SD (n = 3).